

Triphenylamine (TPA)-Functionalized Structural Isomeric Polythiophenes as Dopant Free Hole-Transporting Materials for Tin Perovskite Solar Cells

Rajendiran Balasaravanan, Chun-Hsiao Kuan, Shih-Min Hsu, En-Chi Chang, Yu-Cheng Chen, Yi-Tai Tsai, Meng-Li Jhou, Shueh-Lin Yau, Cheng-Liang Liu, Ming-Chou Chen,* and Eric Wei-Guang Diau*

A new series of triphenylamine (TPA)-functionalized isomeric polythiophenes are developed as hole transporting materials (HTM) for inverted tin-based perovskite solar cells (TPSCs). Bithiophene (BT) is first functionalized with two TPA (electron donor; D) at 3 and 5 positions to give two structural isomeric compounds (3BT2D and 5BT2D). The functionalized BT2Ds are then coupled with 3,3'-bis(tetradecylthio)-2,2'-bithiophene (SBT-14)/3,3'-ditetradecyl-2,2'-bithiophene (BT-14) to produce structural isomeric polythiophenes (1-4), which are compared to conventional poly[N,N"-bis(4-butylphenyl)-N,N"-bis(phenyl)-benzidine] (poly-TPD) as HTMs for TPSCs. With the appropriate alignment of energy levels with regard to the perovskite layer, the TPA-functionalized polymers-based TPSCs exhibit enhanced operational stability and efficiency. Moreover, the long thiotetradecyl chain in SBT-14 with intramolecular S(alkyl)•••S(thio) interactions restricts the molecular rotation and has a strong impact on the molecular solubility and wettability of the film during device fabrication. Among all the polymers studied, TPSCs fabricated with 3-SBT-BT2D polymer exhibit the highest hole mobility as well as the slowest charge recombination and achieve the highest power conversion efficiency of 8.6%, with great long-term stability for the performance retaining ≈90% of its initial values for shelf storage over 4000 h, which is the best efficiency for non-PEDOT:PSS-based TPSCs ever reported.

1. Introduction

The development of organic-inorganic halide perovskites in optoelectronics has attracted much research interest in recent years due to their broad spectra of light absorption with suitable bandgaps, large carrier mobility, and long carrier diffusion lengths.^[1-4] Tin in the B-site played a promising role in the development of high-efficiency solar cells because Sn perovskite has similar optical and electronic properties and crystal structure compared to Pb perovskite.^[5-10] However, the current problem is the moisture and oxygen stability of tin, which limits the development of Sn-based perovskite solar cells (TPSCs) due to the air sensitivity of the tin perovskites. Oxidation of Sn²⁺ to Sn⁴⁺ easily occurs, leading to the formation of uncontrollable p-type doping and a high density of trap states during device fabrication.^[11-18] With regard to overcoming these problems and improving the power conversion efficiency

R. Balasaravanan, E.-C. Chang, Y.-T. Tsai, M.-L. Jhou, S.-L. Yau, M.-C. Chen
Department of Chemistry and Research Center of New Generation Light
Driven Photovoltaic Modules
National Central University
Taoyuan 32001, Taiwan
E-mail: mcchen@ncu.edu.tw
C.-H. Kuan, S.-M. Hsu, Y.-C. Chen, E. W.-G. Diau
Department of Applied Chemistry and Institute of Molecular Science
Center for Emergent Functional Matter Science
National Yang Ming Chiao Tung University
Hsinchu 30010, Taiwan
E-mail: diau@nycu.edu.tw

C.-L. Liu
Department of Materials Science and Engineering
National Taiwan University
Taipei 10617, Taiwan
E. W.-G. Diau
Center for Emergent Functional Matter Science
National Yang Ming Chiao Tung University
Hsinchu 300093, Taiwan

 The ORCID identification number(s) for the author(s) of this article
can be found under <https://doi.org/10.1002/aenm.202302047>

DOI: 10.1002/aenm.202302047

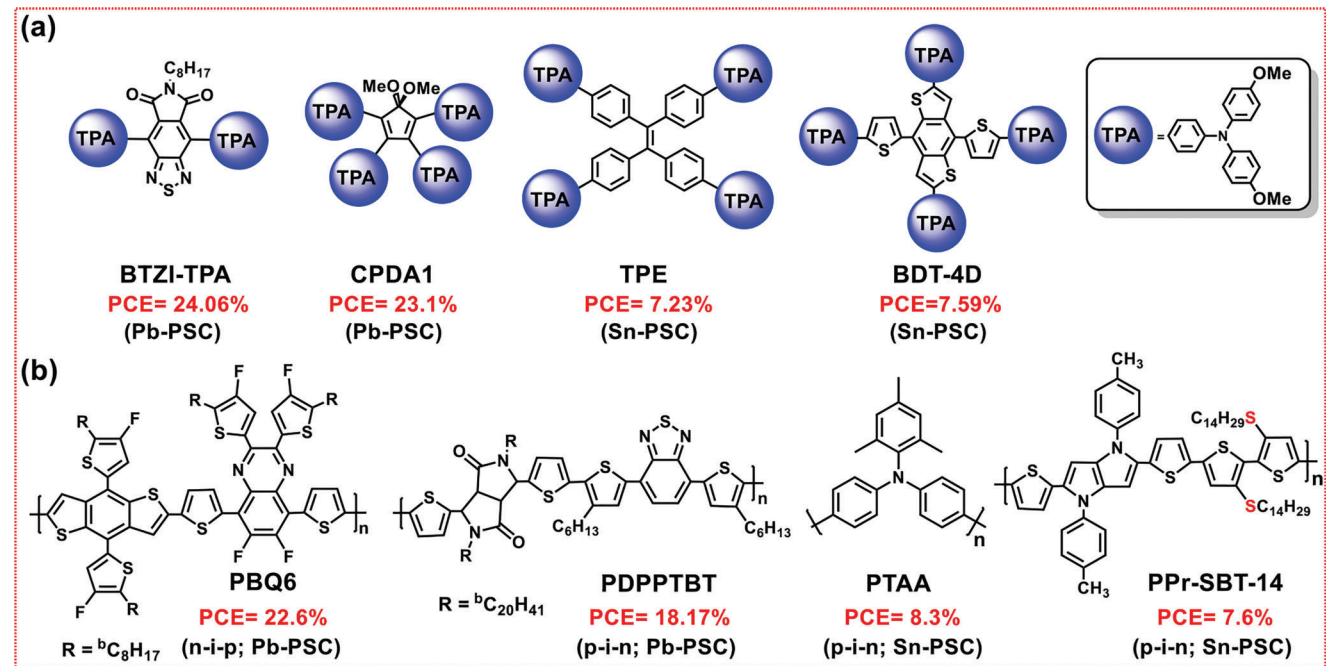


Figure 1. Recent reports of the most efficient dopant-free a) small molecular and b) polymeric HTMs for Pb- and Sn-based PSCs.

(PCE) in TPSCs, p-type semiconductor materials known as hole transport materials (HTMs) have been shown to play an intriguing role in efficient charge separation and transport, and also encourage perovskite film crystallization, which could significantly improve their PCEs.^[19] However, in some cases, dopants have been used to improve the charge transport properties. The doping approaches cause some problems, such as device degradation and morphological defects, which make them unsuitable for scalable production.^[20,21] In addition, most high-performance TPSCs were fabricated using poly(3,4-ethylenedioxythiophene):poly(styrene sulfonate) (PEDOT:PSS) as an HTM. However, the hydroscopic HTM is sensitive to moisture so that the PEDOT:PSS-based TPSC would suffer from the stability problem. To solve these problems, the development of alternative low-cost dopant-free HTMs with excellent hole transport properties is urgently needed.^[22]

To design highly efficient HTM, fused heteroaromatics^[23] with π -conjugated systems, such as, thiophene,^[24] bithiophene,^[25] carbazole,^[26] anthracene,^[27] pyrene,^[28] pyrazine,^[29] and thieno-pyrazine^[30] have been explored as central cores and were functionalized with TPAs. The latter is commonly used as a core or end-capping group for efficient charge extraction and hole transport, which leads to materials with high hole conductivity. As a result, some TPA-functionalized small molecular HTMs have been developed and achieved high PCE in Pb- or Sn-PSC. As shown in Figure 1a, BTZI-TPA^[31] delivered a high efficiency of 24.06% when serving as an interface layer (18.44% PCE as HTM) and CPDA1 achieved efficiencies of 23.1%^[32] as HTM in Pb-PSC. Similarly, TPA-end capped TPE- and BDT-based small molecular HTMs exhibited efficiencies of 7.23% and 7.59% in Sn-PSC.^[33,34] Polymeric HTMs have attracted much interest in recent years due to their good processability in solution to produce continuous and uniform films and their high

electron mobility with low LUMO energy level to enhance the PCE and stability in PSCs.^[35–37] However, the development of highly efficient polymeric HTMs has been quite slow, and the PCEs obtained are much lower than those of small molecular HTMs. For example, the most efficient dopant-free quinoxaline-based polymeric PBQ6^[38] and PDPPTBT^[39] achieved the highest efficiency of 22.6% (n-i-p) and 18.17% (p-i-n) PCE in Pb-based PSCs, respectively, as shown in Figure 1b. At present, new polymeric HTMs have rarely been explored for TPSC, only conventional polymers such as poly[bis(4-phenyl)(2,4,6-trimethylphenyl)amine] (PTAA) or poly[N,N'-bis(4-butylphenyl)-N,N'-bis(phenyl)-benzidine] (poly-TPD) have been examined for Sn-PSCs.

For example, PTAA-based TPSC recently achieved a PCE of 8.3%, which is the first example of a non-PEDOT:PSS-based TPSC.^[40] More recently, a new dopant-free pyrrolopyrrole-conjugated thioalkylated BT-based polymeric HTM (PPr-SBT; as shown in Figure 1b) was developed and a PCE of 7.6% was achieved with an excellent long-term stability over 6000 h in TPSC.^[41] In general, the hydrophobic nature of these polymers made it difficult to deposit the tin perovskite layer and the long-term stability also suffered, and thus the goal of developing highly efficient polymeric HTM with excellent long-term stability for TPSC still seems distant.

Recently, our team has developed a TPA-functionalized BT-based small molecular HTM which exhibited a high 19.34% PCE with exceptional stability (98% in 1186 h) in Pb-PSC.^[24] Further studies on the TPA-functionalized position of the BT core achieved a higher PCE of up to 21.73% along with long stability in Pb-PSC^[42] (structures of both HTMs are shown in Figure 2). With the successful development of the first highly efficient polymeric HTM for TPSC by utilizing the SBT unit,^[41] and the above two TPA-functionalized BT-based small molecular

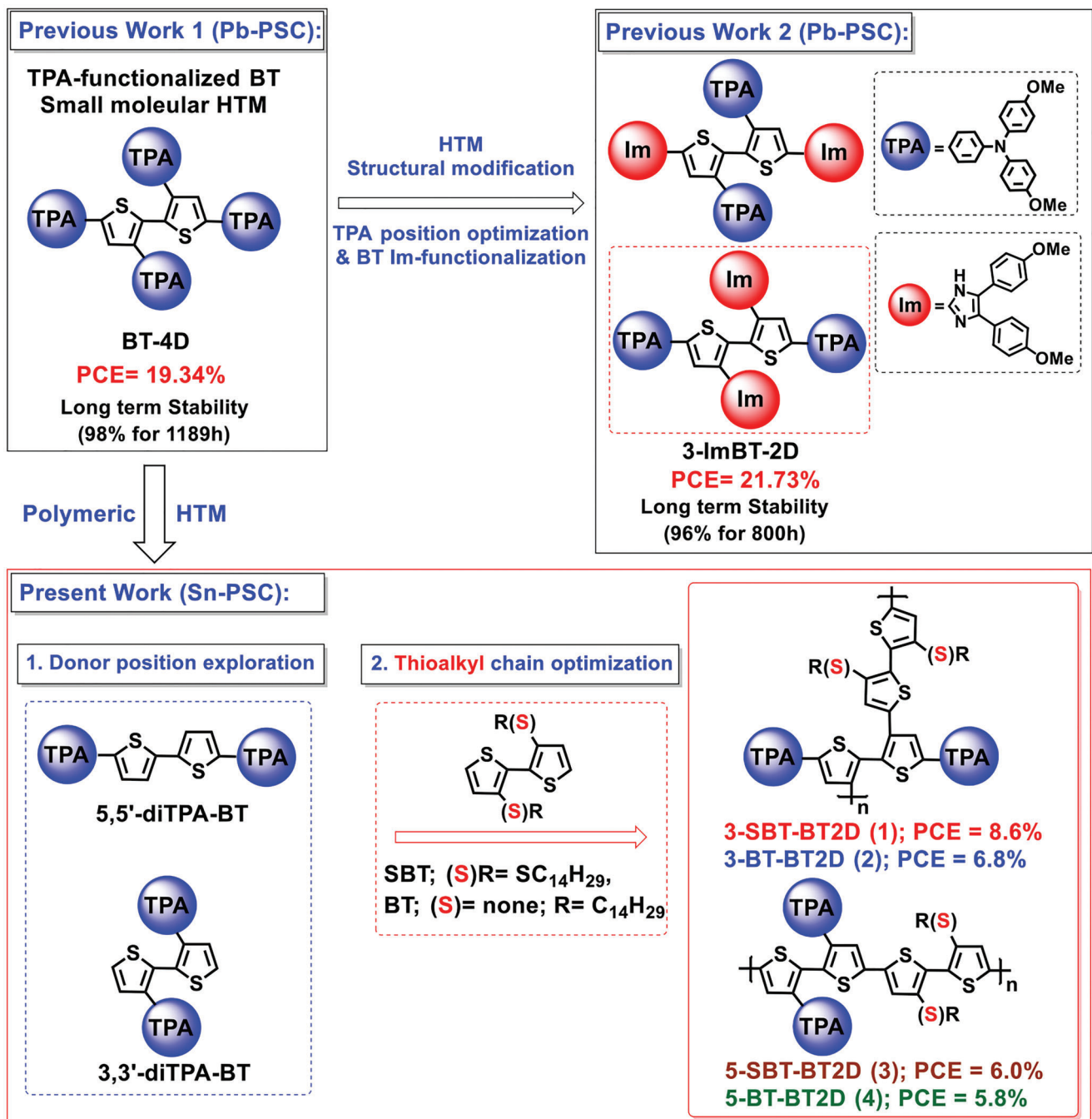
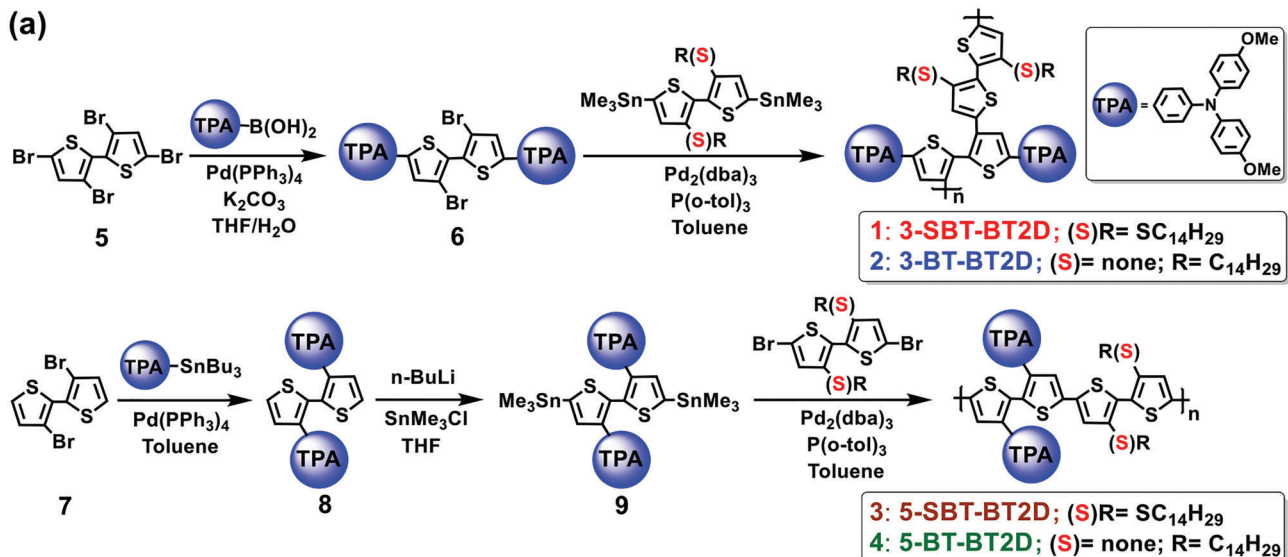


Figure 2. Strategy and Molecular structures of dopant-free polymeric HTMs for p-i-n TPSCs.

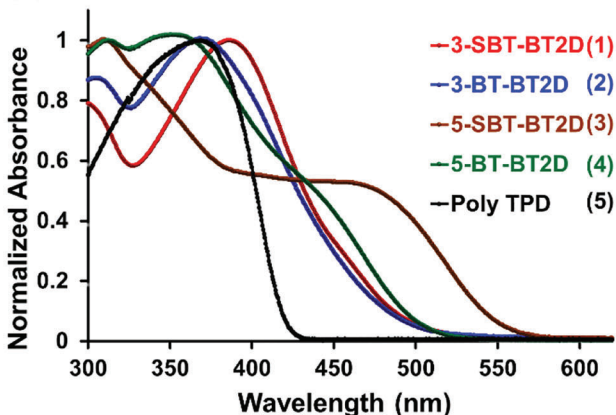
HTMs with long-term stability in Pb-PSC, we envisioned the first TPA-functionalized thioalkylated BT-based polymeric HTM that might accomplish high efficiency with good long-term stability for TPSC. Note, no TPA-functionalized polymers have ever been explored for PSC. Further, we realized the functionalized TPAs in various structural positions in the polymer backbone should strongly affect the molecular conformation, solubility, wettability of the film, and well-matched HOMO level, and thus both the TPA-functionalized structural

isomeric BT units, 3,3'-diTPA-BT and 5,5'-diTPA-BT (structures are shown in Figure 2), were explored. To ensure a more planar structure to avoid disruption of π -conjugation and allow tight intermolecular π - π -stacking, which is essential for good charge transport properties of the materials,^[43,44] the more planar, intramolecular S(alkyl)…S(thiophene) locks possessing SBT unit^[45-50] was utilized as the conjugated unit. Thus, isomeric structural TPA-functionalized BT units were conjugated with the 3,3'-bis(tetradecylthio)-2,2'-bithiophene (SBT-14) unit

(a)



(b)



(c)

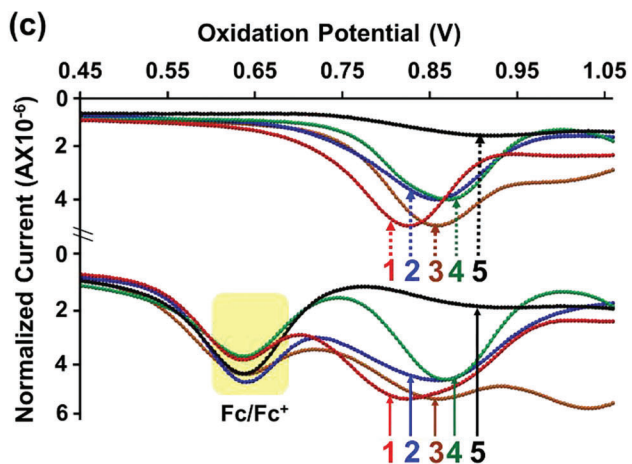


Figure 3. a) Synthetic Route of target polymers. b) Normalized UV-vis absorption spectra of all the polymers in dichlorobenzene solution. c) Normalized differential pulse voltammograms (DPV) of 3-SBT-BT2D (red; 1), 3-BT-BT2D (blue; 2), 5-SBT-BT2D (brown; 3), 5-BT-BT2D (green; 4) and Poly-TPD (black; 5) recorded in $\text{o-C}_6\text{H}_4\text{Cl}_2$ with (bottom part)/without (upper part) addition of ferrocene (as internal standard; calibrated at +0.64 V). The DPV of each polymer is adjusted for clarity.

to give two polymeric HTMs, 3-SBT-BT2D, and 5-SBT-BT2D, for dopant-free TPSC study. For comparison, an alkylated 3,3'-ditetradecyl-2,2'-bithiophene (BT-14) unit is also employed to prepare polymeric 3-BT-BT2D and 5-BT-BT2D (Figure 2). Furthermore, the conventional poly-TPD is also investigated as HTMs for TPSCs for comparison. As foreseen, the thioalkylated TPA-functionalized 3-SBT-BT2D-based device achieves a PCE of 8.6% with long-term stability of over 4000 h, which is the best result ever reported for a non-PEDOT:PSS TPSC.

2. Results and Discussion

The synthetic pathway for four TPA-functionalized polymers is shown in Figure 3a. 3,3',5,5'-tetrabrominated bithiophene (5) and 3,3'-dibrominated bithiophene (7) were prepared accord-

ing to known protocols.^[25] First, compound 5 was successfully selectively Suzuki-coupled with triphenylamine boronic acid to give 5,5'-di-TPA-substituted 3,3'-dibrominated bithiophene (6), which was then Stille-coupled with bis(trimethylstannyl)-SBT(14) or bis(trimethylstannyl)-BT(14)^[41] to afford the target polymers 3-SBT-BT2D (1) and 3-BT-BT2D (2), respectively. Similarly, 3,3'-dibrominated bithiophene (6) was first Stille-coupled with stannylated TPA units to give 3,3'-di-TPA-functionalized bithiophene (7). However, the attempt to brominate the latter to prepare the corresponding dibrominated di-TPA bithiophene was not very successful, and a mixture of some undesired impurities coexisted. Bithiophene (7) was thus deprotonated and then stannylated with trimethyltin chloride to give 3,3'-di-TPA-functionalized distannylated bithiophene (9). Finally, Stille-coupling of compound 9 with di-brominated SBT-14 or

Table 1. Thermal, optical, and electrochemical properties of all the polymers.

Polymers	T_d [°C] ^{a)}	T_m [°C] ^{b)}	λ_{abs} (soln) ^{c)} [nm]	λ_{onset} (soln) ^{d)} [nm]	E_{Ox} [V] ^{e)}	HOMO [eV] ^{e)}	LUMO [eV] ^{e)}	ΔE_g [eV] ^{f)}
3-SBT-BT2D (1)	367.2	108.3	387, 451	503	0.82	-5.26	-2.80	2.46
3-BT-BT2D (2)	376.0	106.8	369	500	0.86	-5.30	-2.82	2.48
5-SBT-BT2D (3)	324.6	107.1	300, 466	554	0.86	-5.30	-3.07	2.23
5-BT-BT2D (4)	413.0	107.5	357, (442)	505	0.87	-5.31	-2.86	2.45
Poly-TPD (5)	n.d. ^{g)}	n.d. ^{g)}	371	422	0.91	-5.35	-2.41	2.94

^{a)} By TGA; ^{b)} Melting point from DSC; ^{c)} Absorption spectra were measured in *o*-C₆H₄Cl₂; ^{d)} Onset absorption; ^{e)} By DPV in *o*-C₆H₄Cl₂, E_{ox} = Oxidative potential; E_{HOMO} = $-(4.44 + 0.64 + E_{ox})$; E_{LUMO} estimated from $E_{HOMO} + E_g$; ^{f)} energy bandgap was calculated by $1240/\lambda_{onset}$; ^{g)} Not determined.

BT-14^[45] afforded the corresponding polymers **5-SBT-BT2D (3)** and **5-BT-BT2D (4)**, respectively. Details of the synthesis of the new compounds can be found in the Supporting Information. All final compounds were thoroughly characterized by ¹H NMR and ¹³C NMR spectroscopies (Figures S1–S11, Supporting Information), and gel permeation chromatography (GPC) analysis (as shown in Figures S12–S15, Supporting Information). The four polymeric HTMs are soluble in common organic solvents, making them accessible for device fabrication by the solution process.

The weight-average molecular weights (Mw) of all four polymers were determined by GPC and exhibited the Mw range from 12.4 to 20 kDa with a dispersity index range of 1.74–2.84. For the polymers 3-SBT-BT2D, 3-BT-BT2D, 5-SBT-BT2D, and 5-BT-BT2D, the respective degrees of polymerization (DPs) are 10, 15.7, 9, and 10, respectively. The DPs are relatively low. The primary reason for the low DP in all these polymers can be attributed to the presence of two bulky TPA moieties within the bithiophene unit. These moieties act as steric hindrances, limiting the potential for higher degrees of polymerization. Nevertheless, the long thio- or nonthio-alkyl chains contribute to a strong hydrophobic effect around the backbone and show a strong influence on the chemical and physical properties of the polymers as well as the deposited tin perovskite thin-film morphology (vide infra).

Thermogravimetric analysis (TGA) and differential scanning calorimetry (DSC) were performed to investigate the thermal properties of the polymers, and the corresponding data are summarized in **Table 1**. As shown in Figure S16 (Supporting Information), all polymers exhibit high decomposition temperatures (T_d at 5% weight loss) at about or above 320 °C in TGA, and the phase transition temperatures of these polymers were observed nearly at 107–108 °C by DSC measurement. Both results indicate that the new polymers are sufficiently thermally stable and possess low crystallinity with high thermal stability in the solid film state.

To find out the optical behavior of these polymers, the absorption spectra of all polymers were recorded in *o*-dichlorobenzene (as shown in Figure 3b), and the corresponding data are organized in Table 1. The absorption maxima of the polymers **3-SBT-BT2D**, **3-BT-BT2D**, **5-SBT-BT2D**, and **5-BT-BT2D** are located at 387, 369, 466, and 357 nm, respectively. The absorption profile is determined by the substitution position of TPAs and is also thio- or nonthio-alkyl chain dependent. For thioalkylated polymers (1 and 3), a red-shifted absorption was observed in comparison to their alkylated analogs (2 and 4), indicating enhanced π -conjugation within the SBT core with core planarization via intramolecular locking (vide infra).^[51] Note that all newly developed

polymers exhibit more red-shifted absorption onset than the conventional poly-TPD, which is attributed to the expansion of π -conjugation in the central scaffold, and this would benefit intramolecular charge transfer.

The HOMO energy levels of the five polymeric HTMs are determined by differential pulse voltammogram (DPV) measurements. As shown in Figure 3c, the oxidation potentials of all five polymers were recorded in *o*-dichlorobenzene solution with Bu₄NPF₆ as the supporting electrolyte and were calibrated using ferrocene as an internal standard, which was set at +0.64 V. The oxidation peaks of polymers 1–5 were calibrated and they exhibited at +0.82, +0.86, +0.86, +0.87, and +0.91 V, respectively (Table 1). The HOMO energy level of each polymer versus NHE is estimated by adding 4.44 eV to the oxidation potential.^[52] The values of the HOMO levels of 1–5 obtained from the oxidation potentials are thus -5.26, -5.30, -5.30, -5.31, and -5.35 eV, respectively. Note, all the new TPA-functionalized polythiophenes possess higher HOMO energies than poly-TPD. As expected, the HOMO of thioalkylated **3-SBT-BT2D (1)** is higher than that of non-thioalkylated **3-BT-BT2D (2)**,^[53] which can be attributed to a stronger planarization of the SBT unit than its BT analog. Similarly, the polymer **5-SBT-BT2D (3)** shows a higher HOMO value compared to its BT-based analog (4). Since the first oxidation occurs in the TPA unit, the position of TPA functionalization also shows a strong influence on the HOMO energies of four polymers. With TPA functionalized at the 5,5' position of bithiophene, the end-capped TPA moieties in 1 feature a better conjugation to the bithiophene backbone than TPA substituted at the 3,3' position. Thus, **3-SBT-BT2D (1)** exhibits the highest HOMO value among the newly developed polymers. The LUMO value of polymers 1–5 was estimated by adding the HOMO and the bandgap values derived from the onsets of the absorption spectra and giving -2.80–2.82, -3.07, -2.86, and -2.41 eV, respectively. All new polymers exhibit HOMOs and LUMOs that are in a suitable energy range and are able to efficiently extract holes from the perovskite film while blocking the reverse electron flow from the perovskite to the ITO back contact electrode.

To study the structural and electronic properties of the polymers, density functional theory (DFT) calculations were performed using Gaussian09 software with the basis set B3LYP/6-31G(d,p) (Figures S17 and S18, Supporting Information). The DFT results show that all polymers (represented by dimers only) exhibit a nearly coplanar preferred conformation. As shown in Figure S17a,b (Supporting Information), the HOMOs of SBT-based polymers exhibit uniform electronic distributions and are well delocalized along the entire molecular backbone of the

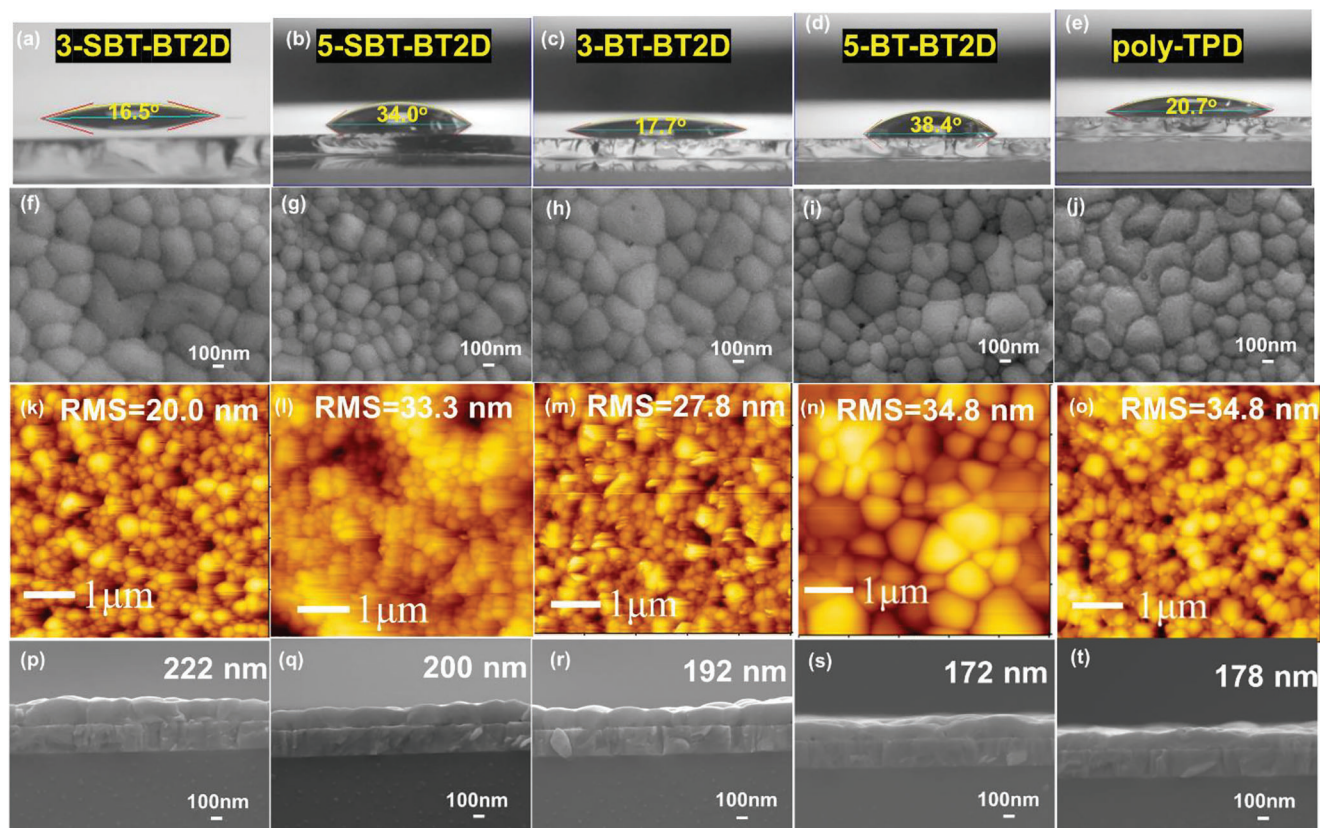


Figure 4. a–e) Contact angles of perovskite precursor SnI_2 , f–j) top-view SEM images of perovskite films, AFM images of perovskite films and Side-view SEM images of perovskite films on varied polymeric HTMs for a,f,k,p) 3-SBT-BT2D b,g,l,q) 5-SBT-BT2D, c,h,m,r) 3-BT-BT2D, d,i,n,s) 5-BT-BT2D, and e,j,o,t) poly-TPD, respectively.

polymers. Note, the dihedral angles of TPAs in the 5,5' position of bithiophene are smaller than those TPAs in 3,3' position due to more steric congestion of the latter. As a result, the calculated HOMO (-4.43 eV) of 3-SBT-BT2D is higher than that of 5-SBT-BT2D (-4.76 eV). This trend is consistent with the electrochemically derived DPV values of these two polymers (-5.26 vs -5.30 eV; *vide infra*). The higher planarity of the backbones in the polymer 3-SBT-BT2D could promote the formation of both intramolecular charge delocalization and π - π -stacking interactions between the polymer backbones in the solid state. Furthermore, SBT-based polymers possess higher HOMOs (-4.43 and -4.76 eV) than their BT-based analogs (-4.99 and -5.03 eV), as expected, which can be attributed to the intramolecular S–S interactions that promote planarization of the polymers. The electronic distributions of the LUMOs of the polymers are mainly localized at the SBT-substituted central bithiophene units, with some of the delocalized molecular orbitals extending to the phenyl ring. The partial overlap of the molecular orbitals could favor hole extraction and transportation. The DFT results also show that the polymer 3-SBT-BT2D could increase the HOMO energy levels and reduce the LUMO energy levels, which is in good agreement with the electrochemical results. The electrostatic potential surfaces (ESP) of the polymers were calculated (Figure S17c,d, Supporting Information) showing the electron-rich property of the polymers. Note, the sulfur atom in the SBT

unit of polymers can also act as a Lewis base to passivate perovskite surface defects and enhance the stability of TPSCs.^[54]

The wettability and crystal morphology of the tin perovskites deposited on these polymeric HTMs are shown in Figure 4. We first made the HTM films on ITO substrate via spin-coating, then the hydrophobic surfaces of HTMs were modified by the anilinium iodide (ANI)^[41] species to make the film surfaces becoming hydrophilic to some extent. Figures 4a–e show the contact angles of SnI_2 precursor solution on thin films of 3-SBT-BT2D (16.5°), 5-SBT-BT2D (34.0°), 3-BT-BT2D (17.7°), 5-BT-BT2D (38.4°) and poly-TPD (20.7°), respectively. After the polymeric HTM films were treated with ANI, the hydrophobicity was significantly improved, which is helpful for deposition of FAI in the second step to make a tin perovskite FASnI_3 showing good film morphology. Our results indicate that the solution processability of the polymers would strongly affect the device performance (to be discussed later), and only the polymers with suitable solution processability exhibit good device performance. Both polymers 3-SBT-BT2D (or 3-BT-BT2D) and 5-SBT-BT2D (or 5-BT-BT2D) exhibit strong intramolecular S(alkyl)…S(thiophene) interactions. Although these polymers are quite similar, the structural positioning of SBT and TPA differs between them. As a result, the polymer 3-SBT-BT2D has a more planar skeleton with enhanced π -conjugation compared to the polymer 5-SBT-BT2D. This enhanced planarity and π -conjugation contribute to the polymer

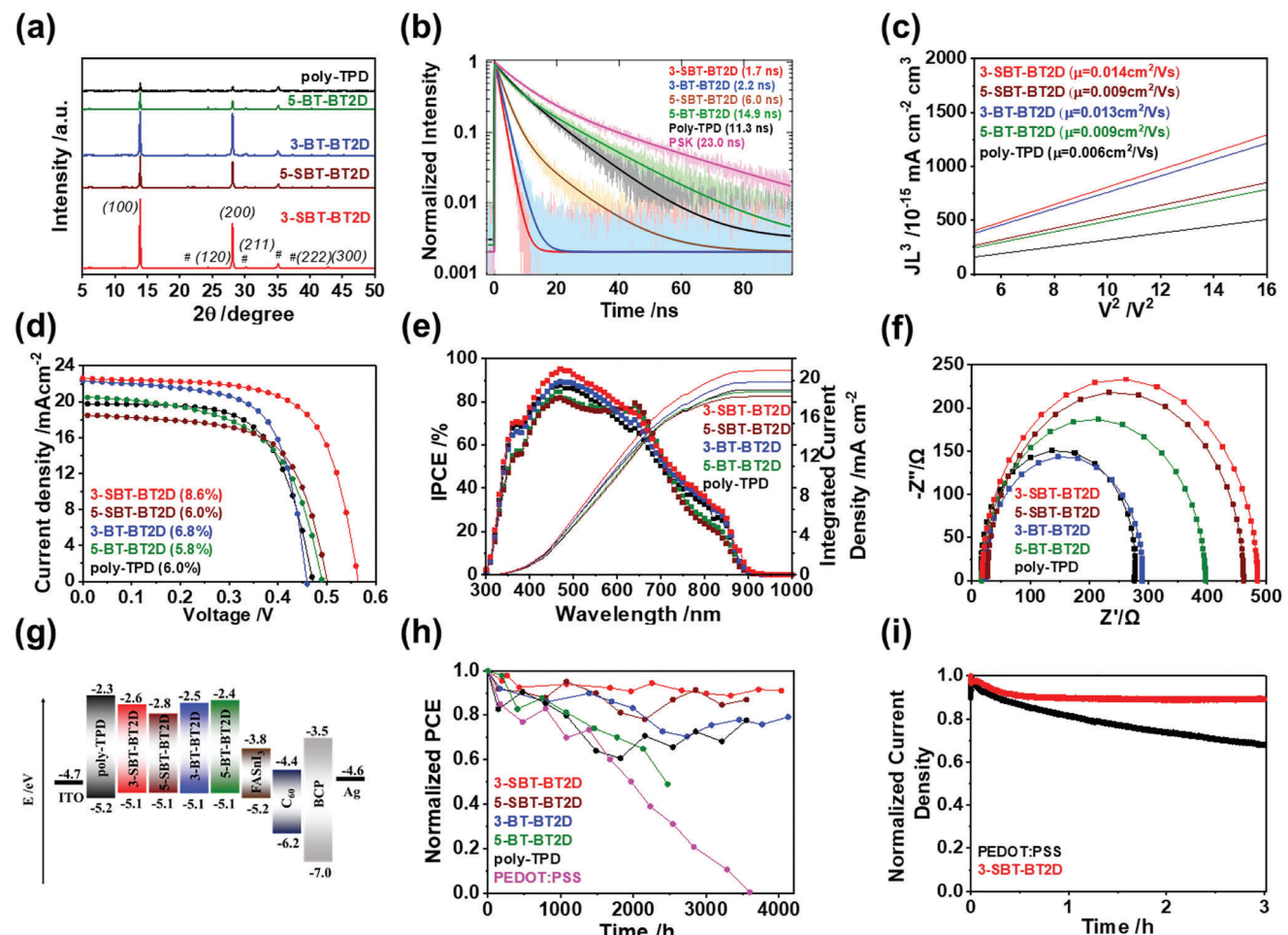


Figure 5. a) XRD, b) PL decay profiles via TCSPC, and c) SCLC of tin perovskites on varied polymeric HTMs as indicated; d) J – V curves, e) IPCE spectra, and f) EIS Nyquist plots for the devices made of tin perovskites deposited on varied polymeric HTMs as indicated; g) energy-level diagram, h) shelf-storage stability, and i) MPP tracking data under light-soaking condition for the devices made of varied polymeric HTMs as indicated. (the best PCE = 8.6%).

3-SBT-BT2D with the much smaller contact angle than that of 5-SBT-BT2D.

Scanning electron microscopy (SEM) and atomic force microscopy (AFM) techniques were used to analyse the morphologies of tin perovskite films fabricated on polymeric HTMs. The AFM images of the polymeric HTMs without and with ANI are shown in Figures S19 and S20 (Supporting Information), respectively. Top-view SEM images of the perovskite films produced on different HTMs are shown in Figures 4f–j. The perovskite films produced on 3-SBT-BT2D exhibit larger and well-arranged crystal grains than the others, which is consistent with the AFM images shown in Figures 4k–o. The AFM images were obtained to investigate the surface roughness of the tin perovskites fabricated on various polymeric HTMs. The results show that the tin perovskite on 3-SBT-BT2D has significantly smaller roughness than the others. Side-view SEM images of the perovskite films produced on various HTMs are shown in Figures 4p–t. Tin perovskite deposited on 3-SBT-BT2D shows greater film thickness (222 nm) than all others, which is expected to give better light harvesting ability than the others.

The XRD patterns of tin perovskites made on different HTMs are shown in Figure 5a, which displays the quality of crystallinity with the order 3-SBT-BT2D > 3-BT-BT2D > 5-SBT-BT2D > 5-BT-BT2D > poly-TPD. In addition, high-resolution GIWAXS images show the good arrangement and crystallization in perovskite at an incident angle of 0.1° in Figure S21 (Supporting Information) for all polymers. Therefore, it is expected that the 3-SBT-BT2D-based device will exhibit better carrier transport property with better device performance than the others. Time-correlated single-photon-counting (TCSPC) measurements were performed to analyze the hole-extraction ability of the tin perovskite films deposited on varied HTMs. The corresponding PL decay profiles (Figure 5b) were obtained with excitation on the glass sides at 635 nm. Only the PL decay profiles of the 3-SBT-BT2D and 3-BT-BT2D films can be fitted with a single-exponential decay function while the other PL transients were fitted with a bi-exponential decay function; the fitted decay coefficients are listed in Table S1 (Supporting Information). The tin perovskite without HTM has an average lifetime of 23.0 ns, and it decreased when HTMs were involved due to the hole-extraction

effect from the VB of perovskite to the HOMO of HTM. The trend of hole-extraction rates shows the order **3-SBT-BT2D** (1.7 ns^{-1}) $>$ **3-BT-BT2D** (2.2 ns^{-1}) $>$ **5-SBT-BT2D** (6.0 ns^{-1}) $>$ **Poly-TPD** (11.3 ns^{-1}) $>$ **5-BT-BT2D** (14.9 ns^{-1}), with the **3-SBT-BT2D** HTM exhibiting the fastest hole-extraction rate. In order to investigate how charge carrier mobility affects photovoltaic performance, we utilized the space-charge limited current (SCLC) method to measure the hole mobilities of the thin films made of these HTMs, and the results are presented in Figure 5c. The structure for the measurement of hole mobility by SCLC is ITO/polymeric HTMs/FASnI₃/Al. The charge mobilities of these HTMs show the order with **3-SBT-BT2D** ($0.014 \text{ cm}^2 \text{ V}^{-1} \text{s}^{-1}$) $>$ **3-BT-BT2D** ($0.013 \text{ cm}^2 \text{ V}^{-1} \text{s}^{-1}$) $>$ **5-SBT-BT2D** ($0.009 \text{ cm}^2 \text{ V}^{-1} \text{s}^{-1}$) $>$ **5-BT-BT2D** ($0.009 \text{ cm}^2 \text{ V}^{-1} \text{s}^{-1}$) $>$ **Poly-TPD** ($0.006 \text{ cm}^2 \text{ V}^{-1} \text{s}^{-1}$), and again **3-SBT-BT2D** shows the best hole mobility among the various HTMs.

Based on the two-step fabrication procedure, the TPSCs can be fabricated with a device structure ITO/HTM/FASnI₃/C60/BCP/Ag. Figure 5d shows the *J*–*V* scan curves for the devices made of polymeric HTMs showing the efficiencies with the order **3-SBT-BT2D** (8.6%) $>$ **3-BT-BT2D** (6.8%) $>$ **5-SBT-BT2D** (6.0%) \approx **Poly-TPD** (6.0%) $>$ **5-BT-BT2D** (5.8%); the photovoltaic parameters are summarized in Table S2 (Supporting Information). The device performance is consistent with the morphology feature demonstrated in Figure 4, whereby the **5-SBT-BT2D** and **5-BT-BT2D** devices exhibited worse performance due to its inferior morphology shown in Figures 4l,n (AFM) and Figures 4g,i (SEM). The **3-SBT-BT2D** device exhibited the best performance (PCE = 8.6%) due to better film morphology and thickness (Figures 4f,k,p), greater crystallinity (Figure 5a), faster hole extraction (Figure 5b) and better hole mobility (Figure 5c) than the others. The IPCE spectra of the BT2D-based devices are presented in Figure 5e, and the integrated *J*_{SC} values are consistent with those obtained from the *J*–*V* curves shown in Figure 5d. The excellent performance of **3-SBT-BT2D** can be attributed to its high *J*_{SC} value, which is reflected in the IPCE spectrum. The enhanced response in the spectral range of 350–500 nm is consistent with the absorption spectrum of **3-SBT-BT2D**, as shown in Figure 3b.

Moreover, the charge recombination properties of the BT2D-based TPSCs were analyzed using electrochemical impedance spectroscopy (EIS) technique, and the results were compared with that of the poly-TPD device. The EIS measurements were conducted in the dark at a bias voltage of 0.5 V. As depicted in Figure 5f, all the Nyquist plots of the devices showed only one semicircle, which was fitted with an RC equivalent circuit model. The fitted impedances indicate the extent of charge recombination, with **3-SBT-BT2D** exhibiting the highest resistance, followed by **5-SBT-BT2D**, **5-BT-BT2D**, **3-BT-BT2D**, and **Poly-TPD**. The charge recombination resistances show the same trend as their respective *V*_{OC} values with the order **3-SBT-BT2D** (0.566 V) $>$ **5-SBT-BT2D** (0.502 V) $>$ **5-BT-BT2D** (0.491 V) $>$ **Poly-TPD** (0.472 V) \approx **3-BT-BT2D** (0.470 V). The superior performance of the **3-SBT-BT2D** device can be attributed to its largest charge recombination resistance, which accounts for its best *V*_{OC} value compared to the other devices. Although the **3-BT-BT2D** device has the lowest *V*_{OC} value confirmed by the EIS results, it has the second-best *J*_{SC} value confirmed by the TCSPC data, making it the second-best device among the others.

To determine the valence band maximum (VBM) energy levels for each HTM, the ultraviolet photoelectron spectroscopy (UPS) measurements were carried out (Figure S22, Supporting Information), while the conduction band minimum (CBM) energy levels were determined using the bandgaps obtained from the UV-vis spectra (Figure S23, Supporting Information). Figure 5g illustrates the energy-level diagram for all the HTMs, along with other relevant species in a TPSC device. The energy levels of the HTMs, as determined by the UPS spectra for the thin-film samples, are higher by \approx 0.2 eV compared to those obtained from the DVP method for the solution samples. Based on the thin-film results, all the HTMs have suitable energy levels to match with that of the tin perovskite, resulting in appreciable device performances, as demonstrated in Figure 5d.

Figure 5h shows the shelf storage stability in the dark for all polymeric TPSCs, including PEDOT:PSS-based TPSC. It has shown that the performance of the PEDOT:PSS-based TPSC gradually degraded upon shelf storage to zero in \approx 3500 h. The poly-TPD device also showed a gradual performance degradation following a trend similar to the device made of PEDOT:PSS within the first 2000 h and then kept stable afterward. The **3-BT-BT2D** device was stable for the first 1500 h but it gradually degraded to 75% of its initial value at 2500 h and remained stable afterward. In contrast, the **3-SBT-BT2D** device exhibited remarkable long-term stability upon shelf storage in a glovebox, with the PCE remaining constant at \approx 90% for over 4000 h. The remarkable optoelectronic properties of **3-SBT-BT2D** make it the best HTM compared to others. To test its reproducibility, the performance statistics (boxplots) of 40 devices with raw data tabulated in Tables S3–S7 (Supporting Information) are shown in Figure S24 (Supporting Information). The effect of hysteresis was evaluated by analyzing the forward and reverse *J*–*V* scans of the **3-SBT-BT2D** device, presented in Figure S25 (Supporting Information). Additionally, the performance of **3-SBT-BT2D** and PEDOT:PSS devices was measured under one sun illumination at the maximum-power point (MPP) in ambient air conditions (\approx 50% relative humidity), as shown in Figure 5i. The MPP measurements demonstrate that an unencapsulated **3-SBT-BT2D** device has an intrinsic light-soaking stability of 3 h, whereas the PCE of the PEDOT:PSS device degraded to 75% of its original performance in 3 h (Figure 5j). Thus, this study introduces a new class of BT2D conducting polymers that can serve as HTMs for TPSCs, with outstanding performance and stability, in particular for the **3-SBT-BT2D** device showing the best PCE (8.6%) as a non-PEDOT:PSS-based TPSC.

3. Conclusion

Four new TPA-functionalized structural isomeric polythiophenes based polymers (**3-SBT-BT2D**, **3-BT-BT2D**, **5-SBT-BT2D**, and **5-BT-BT2D**) were synthesized and used as dopant-free HTMs for inverted TPSCs. The triphenylamine was first functionalized in different positions of bithiophene (**3BT2D** and **5BT2D**) which improved the donating ability of the polymers. The functionalized BT2Ds were coupled with long-chain substituted 3,3'-bis(tetradecylthio)-2,2'-bithiophene (**SBT-14**) / 3,3'-ditetradecyl-2,2'-bithiophene (**BT-14**) to better understand the long chain effect. The new method to combine the TPA functionalization BT2D with the long thio-tetradecyl chain in **SBT-14**

(intramolecular S(alkyl)•••S(thio) interactions) for TPSCs improved the operational stability and film wettability of PSCs. Compared to the reference HTM poly-TPD with the BT2D-based polymers, the BT2D devices showed negligible $J-V$ hysteresis and improved device stability. The performance improvement was attributed to the well-matched energy level, improvement in film morphology, retarded charge carrier recombination, and more efficient extraction of holes from the perovskite layer into the HTM. To the best of our knowledge, the TPSC device fabricated using **3-SBT-BT2D** as HTM exhibited the highest power conversion efficiency of 8.6%, with the device stability over 90% of the original PCE for ≈ 4000 h without encapsulation, which is a new record for a non-PEDOT:PSS TPSC. This work provides a potential strategy to develop a dopant-free polymeric HTM with different isomeric structure for high-efficiency and stable TPSCs.

Supporting Information

Supporting Information is available from the Wiley Online Library or from the author.

Acknowledgements

R.B. and C.-H.K. contributed equally to this work. The authors thank Prof. C.-S. Lin and Ms. Y.-T. Lee of Instrumentation Centre, National Taiwan University for FEG-SEM experiments. The authors also thank Dr. Y.-W. Tsai and Dr. J.-M. Lin (TPS 25A1 NSRRC) for their kind assistance in GIWAXS data analysis. M.-C.C. thanks the financial support provided by the Ministry of Science and Technology of Taiwan (MOST) (MOST-111-2113-M-008-004-MY3 and NSTC-111-2622-8-008-006) and NCU-Covestro Research Center. E.W.-G.D. thanks the support of the National Science and Technology Council (NSTC), Taiwan (grant no. NSTC 111-2634-F-A49-007, NSTC 111-2123-M-A49-001 and NSTC 112-2639-M-A49-001-ASP) and the Centre for Emergent Functional Matter Science of National Yang Ming Chiao Tung University (NYCU) from The Featured Areas Research Centre Program within the framework of the Higher Education Sprout Project by the Ministry of Education (MOE) in Taiwan.

Conflict of Interest

The authors declare no conflict of interest.

Data Availability Statement

The data that support the findings of this study are available in the supplementary material of this article.

Keywords

polymeric hole transporting materials, power conversion efficiency, thioalkylated bithiophenes, tin perovskite solar cells, triphenylamine

Received: June 28, 2023

Revised: July 27, 2023

Published online:

[1] C. C. Stoumpos, M. G. Kanatzidis, *Acc. Chem. Res.* **2015**, *48*, 2791.

- [2] M. Q. Lyu, J.-H. Yun, P. Chen, M. M. Hao, L. Z. Wang, *Adv. Energy Mater.* **2017**, *7*, 1602512.
- [3] S. N. Afraj, D. Zheng, A. Velusamy, W. Ke, S. Cuthriell, X. Zhang, Y. Chen, C. Lin, J.-S. Ni, M. R. Wasielewski, W. Huang, J. S. Yu, C.-H. Pan, R. D. Schaller, M.-C. Chen, M. G. Kanatzidis, A. Facchetti, T. J. Mark, *ACS Energy Lett.* **2022**, *7*, 2118.
- [4] S. N. Afraj, A. Velusamy, C.-Y. Chen, J.-S. Ni, Y. Ezhumalai, C.-H. Pan, K.-Y. Chen, S.-L. Yau, C.-L. Liu, C.-H. Chiang, C.-G. Wu, M.-C. Chen, *J. Mater. Chem. A* **2022**, *10*, 11254.
- [5] F. Bai, Y. Hu, Y. Hu, T. Qiu, X. Miao, S. Zhang, *Sol. Energy Mater. Sol.* **2018**, *184*, 15.
- [6] Y. Hu, S. Zhang, X. Miao, L. Su, F. Bai, T. Qiu, J. Liu, G. Yuan, *Adv. Mater. Interfaces* **2017**, *4*, 1700131.
- [7] W. Ke, C. C. Stoumpos, M. G. Kanatzidis, *Adv. Mater.* **2019**, *31*, 1803230.
- [8] W. Ke, C. C. Stoumpos, I. Spanopoulos, M. Chen, M. R. Wasielewski, M. G. Kanatzidis, *ACS Energy Lett.* **2018**, *3*, 1470.
- [9] Q. Tai, X. Guo, G. Tang, P. You, T.-W. Ng, D. Shen, J. Cao, C.-K. Liu, N. Wang, Y. Zhu, C.-S. Lee, F. Yan, *Angew. Chem., Int. Ed.* **2019**, *58*, 806.
- [10] A. Toshniwal, V. Kheraj, *Sol. Energy* **2017**, *149*, 54.
- [11] Z. Zhu, X. Jiang, D. Yu, N. Yu, Z. Ning, Q. Mi, *ACS Energy Lett.* **2022**, *7*, 2079.
- [12] N. Wang, Y. Zhou, M.-G. Ju, H. F. Garces, T. Ding, S. Pang, X. C. Zeng, N. P. Padture, X. W. Sun, *Adv. Energy Mater.* **2016**, *6*, 1601130.
- [13] T. Leijtens, R. Prasanna, A. Gold-Parker, M. F. Toney, M. D. McGehee, *ACS Energy Lett.* **2017**, *2*, 2159.
- [14] M. A. Kamarudin, D. Hirotani, Z. Wang, K. Hamada, K. Nishimura, Q. Shen, T. Toyoda, S. Iikubo, T. Minemoto, K. Yoshino, S. Hayase, *J. Phys. Chem. Lett.* **2019**, *10*, 5277.
- [15] W. Ke, M. G. Kanatzidis, *Nat. Commun.* **2019**, *10*, 965.
- [16] J. Liu, H. Yao, S. Wang, C. Wu, L. Ding, F. Hao, *Adv. Energy Mater.* **2023**, *13*, 2300696.
- [17] G. Zeng, D. Pu, L. Huang, H. Guan, S. Zhou, J. Zhou, W. Shen, G. Li, G. Fang, W. Ke, *J. Mater. Chem. A* **2023**, *11*, 11245.
- [18] X. Jiang, F. Wang, Q. Wei, H. Li, Y. Shang, W. Zhou, C. Wang, P. Cheng, Q. Chen, L. Chen, Z. Ning, *Nat. Commun.* **2020**, *11*, 1245.
- [19] M. Kyeong, J. Lee, K. Lee, S. Hong, *ACS Appl. Mater. Interfaces* **2018**, *10*, 123254.
- [20] W. Chen, H. Sun, Q. Hu, A. B. Djurisic, T. P. Russell, X. Guo, Z. He, *ACS Energy Lett.* **2019**, *4*, 2535.
- [21] C. Liu, M. Cai, Y. Yang, Z. Arain, Y. Ding, X. Shi, P. Shi, S. Ma, T. Hayat, A. Alsaedi, J. Wu, S. Dai, G. Cao, *J. Mater. Chem. A* **2019**, *7*, 11086.
- [22] D. Song, S. Narral, M.-Y. Li, J.-S. Lin, E. W.-G. Diau, *ACS Energy Lett.* **2021**, *6*, 4179.
- [23] A. Velusamy, S. N. Afraj, S. Yau, C.-L. Liu, Y. Ezhumalai, P. Kumaresan, M.-C. Chen, *J. Chin. Chem. Soc.* **2022**, *69*, 1253.
- [24] T. Krishnamoorthy, F. Kunwu, P. P. Boix, H. Li, T. M. Koh, W. L. Leong, S. Powar, A. Grimsdale, M. Grätzel, N. Mathews, S. G. Mhaisalkar, *J. Mater. Chem. A* **2014**, *2*, 6305.
- [25] V. Joseph, A. A. Sutanto, C. Igci, O. A. Syzgantseva, V. Jankauskas, K. Rakstys, V. I. E. Queloz, H. Kanda, P.-Y. Huang, J.-S. Ni, S. Kinge, M.-C. Chen, M. K. Nazeeruddin, *Small* **2021**, *17*, 2100783.
- [26] A. A. Sutanto, V. Joseph, C. Igci, O. A. Syzgantseva, M. A. Syzgantseva, V. Jankauskas, K. Rakstys, V. I. E. Queloz, P.-Y. Huang, J.-S. Ni, S. Kinge, A. M. Asiri, M.-C. Chen, M. K. Nazeeruddin, *Chem. Mater.* **2021**, *33*, 3286.
- [27] X. Liu, F. Kong, R. Ghadari, S. Jin, T. Yu, W. Chen, G. Liu, Z. Tan, J. Chen, S. Dai, *Chem. Commun.* **2017**, *53*, 9558.
- [28] N. J. Jeon, J. Lee, J. H. Noh, M. K. Nazeeruddin, M. Grätzel, S. I. Seok, *J. Am. Chem. Soc.* **2013**, *135*, 19087.
- [29] G. Xu, R. Xue, M. Zhang, Y. Li, Y. Li, *Acta Phys.-Chim. Sin.* **2021**, *37*, 2008050.
- [30] S. C. Rasmussen, R. L. Schwiderski, M. E. Mulholland, *Chem. Commun.* **2011**, *47*, 11394.

[31] X. Ji, K. Feng, S. Ma, J. Wang, Q. Liao, Z. Wang, B. Li, J. Huang, H. Sun, K. Wang, X. Guo, *ACS Nano* **2022**, *16*, 11902.

[32] M. Bauer, H. Zhu, T. Baumeler, Y. Liu, F. T. Eickemeyer, C. Lorenz, E. Mena-Osteritz, D. Hertel, S. Olthof, S. M. Zakeeruddin, K. Meerholz, M. Grätzel, P. Bäuerle, *Adv. Energy Mater.* **2021**, *11*, 2003953.

[33] S. Vegiraju, W. Ke, P. Priyanka, J.-S. Ni, Y.-C. Wu, I. Spanopoulos, S. L. Yau, T. J. Marks, M.-C. Chen, M. G. Kanatzidis, *Adv. Funct. Mater.* **2019**, *29*, 1905393.

[34] W. Ke, P. Priyanka, S. Vegiraju, C. C. Stoumpos, I. Spanopoulos, C. M. M. Soe, T. J. Marks, M.-C. Chen, M. G. Kanatzidis, *J. Am. Chem. Soc.* **2018**, *140*, 388.

[35] M. Statz, S. Schneider, F. J. Berger, L. Lai, W. A. Wood, M. Abdi-Jalebi, S. Leingang, H.-J. Himmel, J. Zaumseil, H. Sirringhaus, *ACS Nano* **2020**, *14*, 15552.

[36] P.-S. Lin, S. Inagaki, J.-H. Liu, M.-C. Chen, T. Higashihara, C.-L. Liu, *Chem. Eng. J.* **2023**, *458*, 141366.

[37] M. M. H. Desoky, M. Bonomo, N. Barbero, G. Viscardi, C. Barolo, P. Quagliotto, *Polymers* **2021**, *13*, 1652.

[38] C. Lu, C. Zhu, L. Meng, C. Sun, W. Lai, S. Qin, J. Zhang, W. Huang, J. Du, Y. Wang, Y. Liu, *Sci. China Chem.* **2021**, *64*, 2035.

[39] S. Guo, X. Zhang, Z. Li, Y.-M. Chen, H. Wang, Y. Hao, *RRL Solar* **2021**, *5*, 2100506.

[40] C.-H. Kuan, G. S. Luo, S. Narra, S. Maity, H. Hiramatsu, Y.-W. Tsai, J.-M. Lin, C.-H. Hou, J.-J. Shyue, E. W.-G. Diau, *Chem. Eng. J.* **2022**, *450*, 138037.

[41] C.-H. Kuan, R. Balasaravanan, S.-M. Hsu, J.-S. Ni, Y.-T. Tsai, Z.-X. Zhang, M.-C. Chen, E. W.-G. Diau, *Adv. Mater.* **2023**, *35*, 2300681.

[42] J. X. Xia, V. Joseph, A. A. Sutanto, R. Balasaravanan, Y. Ezhumalai, Z.-X. Zhang, J.-S. Ni, S. T. Yogesh, S.-L. Yau, G. Shao, Z. Qiu, A. M. Asiri, M.-C. Chen, M. K. Nazeeruddin, *Cell Rep. Phy. Sci.* **2023**, *4*, 101312.

[43] H. Chen, Y. Guo, G. Yu, Y. Zhao, J. Zhang, D. Gao, H. Liu, Y. Liu, *Adv. Mater.* **2012**, *24*, 4618.

[44] C. Wang, Y. Qin, Y. Sun, Y.-S. Guan, W. Xu, D. Zhu, *ACS Appl. Mater. Interfaces* **2015**, *7*, 15978.

[45] S. Vegiraju, B.-C. Chang, P. Priyanka, D.-Y. Huang, K.-Y. Wu, L.-H. Li, W.-C. Chang, Y.-Y. Lai, S.-H. Hong, B.-C. Yu, C.-L. Wang, W.-J. Chang, C.-L. Liu, M.-C. Chen, A. Facchetti, *Adv. Mater.* **2017**, *29*, 1702414.

[46] E. Salatelli, M. Marinelli, M. Lanzi, A. Zanelli, S. Dell'Elce, A. Liscio, M. Gazzano, F. Di Maria, *J. Phys. Chem. C* **2018**, *122*, 4156.

[47] Z. Xue, S. Chen, N. Gao, Y. Xue, B. Lu, O. A. Watson, L. Zang, J. Xu, *Polym. Rev.* **2020**, *60*, 318.

[48] S. N. Afraj, C.-C. Lin, A. Velusamy, C.-H. Cho, H.-Y. Liu, J. Chen, G.-H. Lee, J.-C. Fu, J.-S. Ni, S.-H. Tung, S. Yau, C.-L. Liu, M.-C. Chen, A. Facchetti, *Adv. Funct. Mater.* **2022**, *32*, 2200880.

[49] H. Huang, L. Yang, A. Facchetti, T. J. Marks, *Chem. Rev.* **2017**, *117*, 10291.

[50] C.-C. Lin, S. N. Afraj, A. Velusamy, P.-C. Yu, C.-H. Cho, J. Chen, Y. H. Li, G.-H. Lee, S.-H. Tung, C.-L. Liu, M.-C. Chen, A. Facchetti, *ACS Nano* **2021**, *15*, 727.

[51] S. Vegiraju, X.-L. Luo, L.-H. Li, S. N. Afraj, C. Lee, D. Zheng, H.-C. Hsieh, C.-C. Lin, S.-H. Hong, H.-C. Tsai, G.-H. Lee, S.-H. Tung, C.-L. Liu, M.-C. Chen, A. Facchetti, *Chem. Mater.* **2020**, *32*, 1422.

[52] V. Joseph, J. Xia, A. A. Sutanto, V. Jankauskas, C. Momblonia, B. Ding, K. Rakstys, R. Balasaravanan, C.-H. Pan, J.-S. Ni, S.-L. Yau, M. Sohail, M.-C. Chen, P. J. Dyson, M. K. Nazeeruddin, *ACS Appl. Mater. Interfaces* **2022**, *14*, 22053.

[53] Y. Ezhumalai, F.-S. Lin, M.-S. Fan, K. Prabakaran, J.-S. Ni, Y.-C. Wu, G.-H. Lee, M.-C. Chen, K.-C. Ho, *ACS Appl. Mater. Interfaces* **2020**, *12*, 15071.

[54] Y. Li, S. C. Duan, L. Z. Zhang, Y. Zhang, Z. Tang, B. Xu, *ACS Appl. Energy Mater.* **2021**, *4*, 3526.